ANALYSES OF VECTOR MAGNETOGRAMS

JINGXIU WANG
Beijing Astronomical Observatory, Chinese Academy of Sciences

ABSTRACT   (1) Current techniques may now permit an acceptable res-
olution of the 180 degree ambiguity in determining the direction of trans-
verse fields. (2) The non-potentiality of active regions can be described by
parameters of angular shear, source field, line-of-sight current, force-free
factor and force-free current. A 2-dimensional description of angular shear
is necessary, and an alternative, FFT method of calculating the line-of-
sight current seems recommendable. (3) For a sampling region, the degree
of non-potentiality quantified by all the parameters shows great enhance-
ment right before a 1M flare, and reduces somehow during the flare. (4) A
highly intermittent distribution of force-free factor with fully mixed signs
is obtained, consistent with a theoretical approach.

INTRODUCTION

Measurements of solar vector magnetic fields are of particular significance with
regard to the studies of solar activities (Hagyard, 1990). The earliest map-
ping of vector magnetic fields was made by Dollfus (1950). A pioneer work of
vector magnetic field measurements was done by Severny and his colleagues at
Crimean Astrophysical Observatory from 1960's to 1970's. Since early 1980's,
great achievement in measurements and analyses of vector magnetic fields, as
well as in understanding the non-potentiality of active regions has been obtained
by Hagyard and her co-workers at Marshall Space Flight Center.

Now a number of new vector magnetographs and Stokes polarimeters are
operated by many groups, such as Huairou (Ai and Hu, 1986, Ming et al. 1988),
Big Bear (Cacciani, Varsik and Zirin, 1989), Mees (Mickey and Canfield, 1989),
Sac Peak (O'Byrne, Rust and Harris, 1989), HAO (Lites et al., 1993), Lockheed
(Title, 1993), Mitaka (Ichimoto et al., 1993) and so on. It seems timely to
exchange ideas and results in vector magnetogram analyses.

In this paper, current techniques and results in analyses of vector mag-
netograms are briefly reviewed, and various approaches are tested with a time
sequence of vector magnetograms obtained at Huairou Solar Observing Station
(HSOS) for an active region.

OBSERVATIONS OF THE VECTOR FIELD AT HSOS

Measurements of the vector magnetic field at Huairou have been made on a daily
basis since 1988 (Ai et al., 1990). Vector magnetic fields of approximately 100

regions per year are mapped with the Solar Magnetic Field Telescope at HSOS. Among them, approximately 40 regions are mapped for more than 4 days. Thus a great source of time sequences of vector magnetograms is available.

The calibration of Huairou magnetograms is based on the relations calculated for some empirical atmospheric models:

$$B_l = C_l \cdot \frac{V}{I}$$
$$B_t = C_t \cdot (\frac{Q^2}{I^2} + \frac{U^2}{I^2})^{\frac{1}{4}}$$

(1)

where the I, V, Q and U are the Stokes parameters transmitted by the filter. The calibration for the line-of-sight component is also empirically examined, like Shi, Wang and Patterson (1986) did for the Big Bear system.

Usually, a 2"×2" smooth-average is made; after that, the noise level for the line-of-sight magnetogram with 255 frame-pair integrations is ∼ 10 gauss; for the transverse magnetogram with the same integrations, ≤50 gauss at the 3 σ level.

METHODS OF REMOVING THE 180 DEGREE AMBIGUITY

1. The Nature of the Ambiguity

The 180 degree ambiguity in determining the transverse field direction is a serious barrier to an accurate understanding of the non-potentiality of active regions. Harvey (1969) is the first author who thoroughly considered this problem. Reviews on this were given by Aly(1989), Gary and Hagyard (1990).

It should be emphasized that the ambiguity is an intrinsic defect of Zeeman measurements. The only way to resolve this ambiguity is to introduce an additional constraint on the field azimuth either from other theoretical considerations, or from independent observations.

A strategy of removing this ambiguity might be recommended. First, a basic resolution can be obtained by an objective method from theoretical considerations, such as the potential field approximation (Harvey, 1969; Sakurai et al., 1985), the force-free approximation (Krall et al., 1982; Wu, 1993), or the divergence-free constraint (Harvey, 1969; Wu and Ai, 1991). Secondly, the resolution should be corrected by more decisive constraints from independent observations, such as H_α fibrils, sunspot penumbra or superpenumbra, as well as the history of the field evolution. Usually, a synthesized means (Wang and Lin, 1993), or a multi-step strategy (Canfield et al., 1992) are required for a satisfactory resolution of the ambiguity.

2. An Alternative Way to Remove the Ambiguity

Gary et al. (1987), Gary and Hagyard (1990) resolved the ambiguity by assuming that the transverse field flowed away from (to) local positive (negative) fields. This can be modified to an objective method. It is assumed that at each pixel in the magnetogram there is a magnetic charge with strength B_l. To determine the transverse azimuth, a unit test charge is introduced at a given point. The net Coulomb's force, $\vec{F}_c$, felt by the test charge from nearby charges, say within 5 to 10 arcsec, would specify the transverse azimuth by
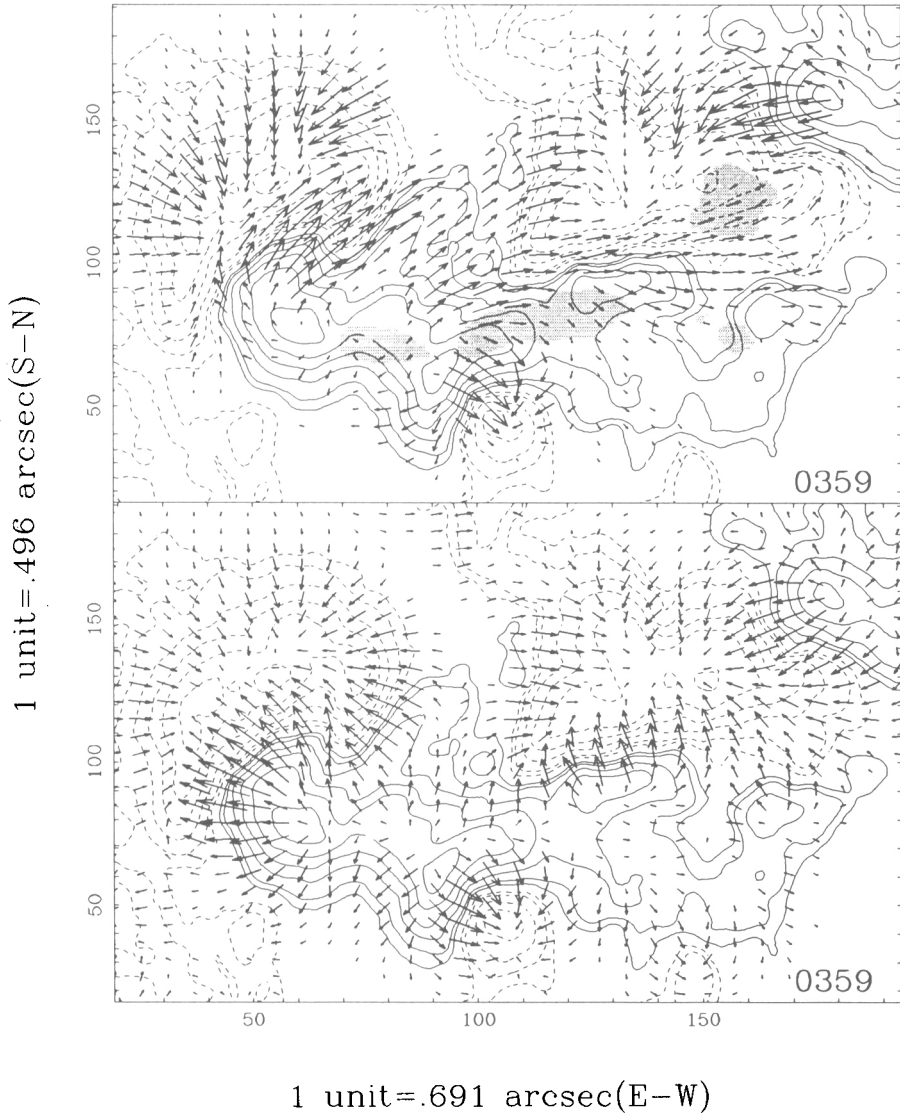
$$\vec{B}_t \cdot \vec{F}_c > 0.$$

(2)

Fig. 1. An ambiguity-removed vector magnetogram (upper part) in comparison with the potential configuration extrapolated from the observed line-of-sight field. The transverse field is represented by arrows with the length proportional to the relative field strength. The line-of-sight field is represented by isogauss contours with solid (dashed) line for positive (negative) polarity. The contour levels are ±160, 320, 640, 960, 1280, and 1600 gauss. Flare ribbons are superposed by grey patches.

The way of adopting magnetic charges and Coulomb's Law is equivalent to the potential field approximation. However, as only the field of a surrounding area is used in the calculation, the local distortion of the global field is taken into account. Therefore, the method is valid for the case of strong magnetic shear. The primary resolution is corrected by the topology constraints revealed from independent observations using an interactive computer program.

The final resolution seems to be fairly satisfactory. In Figure 1, an example of a vector magnetogram of AR 6233 on August 30, 1990 with ambiguity-removed azimuth is shown in comparison with the potential configuration extrapolated from the observed line-of-sight field. The line-of-sight component is represented by isogauss contours with solid (dashed) lines for positive (negative) polarity. The contour levels are ±160, 320, 640, 960, 1280, 1600 gauss. The transverse component is represented by arrows with length proportional to the field strength. The grey patches superposed are H_β flare ribbons at the closest time of the magnetograms.

NON-POTENTIALITY OF ACTIVE REGIONS

1. Angular Shear $\Delta\phi$ and Source Field B_s

To extract the non-potentiality of magnetic field is a central task of vector magnetogram analyses.

One well-known non-potential parameter is the angular shear, $\Delta\phi$, defined by Hagyard et al. (1984). The angular shear is unique because of its independence of the calibration. It is better to retain this uniqueness, and not to weight the angular shear with other uncertain quantities. In previous studies, only the angular shear on the magnetic neutral line is considered, and the observed azimuths are often chosen so that $|\Delta\phi| < 90°$. However, by definition the shear obviously has a 2-D distribution, and its values can extend much beyond ±90 degrees.

The time sequence of angular shear of AR 6233 from 01:00 to 05:07 UT of August 30 is shown on the left of Figure 2. Zones of strong magnetic shear with $|\Delta\phi| > 85°$ are presented by thick iso-shear contours with dashed (solid) lines for negative (positive) angular shear. The line-of-sight fields are shown by only ±250 gauss contours to emphasize the gross magnetic structure. Flare ribbons are superposed as grey patches.

The following results are revealed.

(1). Strong shear zones extend from the neutral line to both sides. A dominant negative sign is found.

(2). One of the earliest brightenings of the 1M flare, indicated by an arrow, appears at the site within a zone of strong shear. Flare ribbons later take place on outer sides, or bracket strong shear zones.

(3). The shear achieves its maximum development with an extreme value of approximately ±160 degrees and its largest area in the earliest phase of the 1M flare; while in the late phase, the relevant strong shear zones are separated into rather smaller pieces and reduced in area slightly.

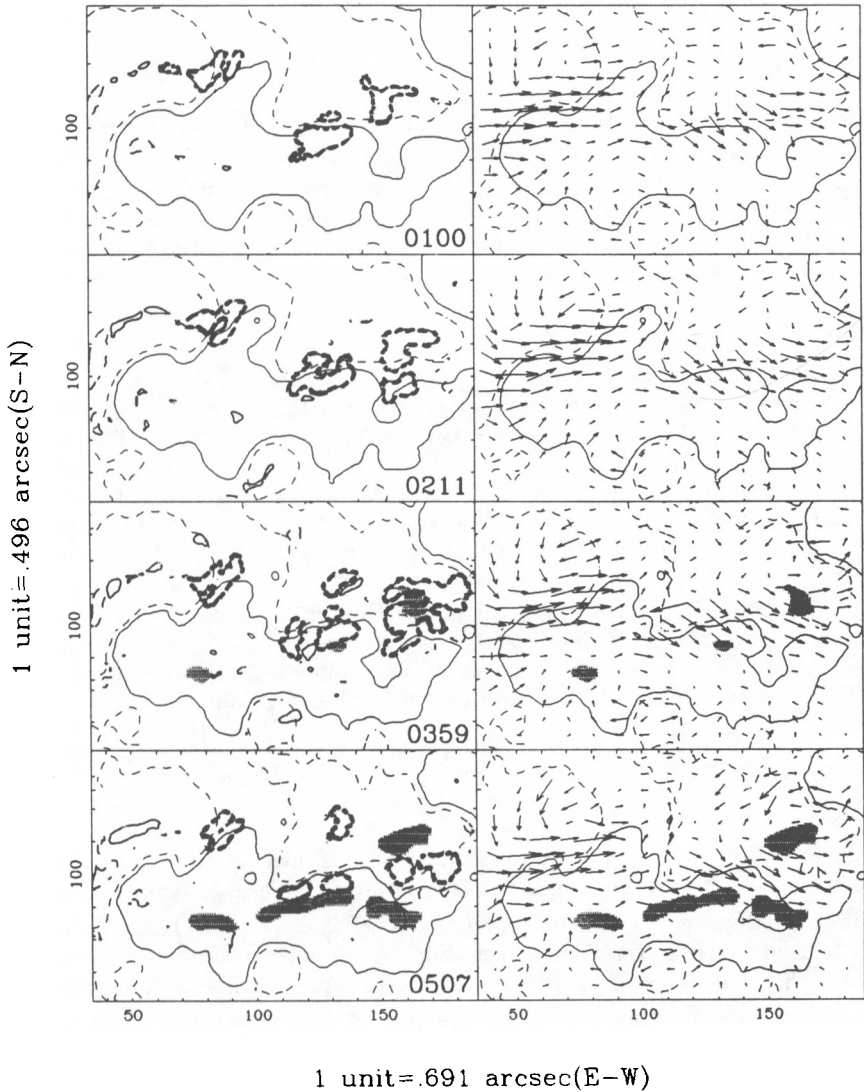A parameter related to the angular shear is the source field which is defined

Fig. 2.   Time sequences of angular shear (on the left) and source field (on the right). Zones of strong magnetic shear with $|\Delta\phi| > 85°$ are presented by thick iso-shear contours with dashed (solid) line for negative (positive) angular shear. The line-of-sight fields are shown by only ±250 gauss contours. Flare ribbons are superposed as grey patches.

by Hagyard et al. (1981) as the vector difference between the observed transverse field and the calculated potential one based on the boundary condition of the line-of-sight field. The source field and angular shear are related by

$$tg(\Delta \phi) = B_{ys}^* - B_{xs}^* \tag{3}$$

where B_{xs}^* and B_{ys}^* are the weighted x, y components of the source field.

The deduced source field of the sampling active region is illustrated on the right of Figure 2 together with the observed line-of-sight magnetic field and the flare ribbons. Two bundles of strong source field are identified. As expected, each bundle of strong source fields corresponds to a set of strong shear zones. Flares do take place on both sides of the bundles of strong source field.

2. Line-of-Sight Current J_z

The line-of-sight current has been extensively studied (Moreton and Severny, 1968; Krall et al., 1982; Deloach et al., 1984; Hagyard et al., 1985; Haisch et al., 1986; Ding et al., 1987; Lin and Gaizauskas, 1987; Hagyard, 1988; Chen and Zhang, 1992; Lin, Wei and Zhang, 1993; Canfield et al., 1991, 1992; Leka et al., 1992; de La Beaujardière, Canfield and Leka, 1992). Generally speaking, some degree of correlations between the location of line-of-sight current concentrations and various manifestations of solar activity is plainly revealed. Canfield et al. (1992) elucidated the physics of the correlations.

The line-of-sight current is calculated from numerical derivatives of the observed transverse field which has a relatively large noise level. The numerical derivatives of noisy data become even noisier and highly uncertain when adopting different numerical methods. However, in the Fourier domain,

$$\hat{J}_z(m,n,z) = \hat{B}_y(m,n,z)[\frac{l \cdot sin(\frac{2\pi m}{I})}{\mu h_x}] - \hat{B}_x(m,n,z)[\frac{l \cdot sin(\frac{2\pi n}{J})}{\mu h_y}] \tag{4}$$

where, $\hat{B}_x$, $\hat{B}_y$ and $\hat{J}_z$ are the relevant Fourier transformations, m,n are Fourier variables, h_x, h_y are distances between adjacent pixels, I, J are dimensions of the magnetograms in x and y directions, and $l = (-1)^{\frac{1}{2}}$. Then, J_z is readily calculated by the reverse transformation. As direct derivatives are avoided and the high frequency noise is reduced, this technique seems recommendable.

The current images deduced are rich in fine structures. The maximum current is found at 04:00 UT, the earliest phase of the major flare. It is as strong as 1.1×10^5 A km^{-2}. The current evolution is shown on the left of Figure 3 with bright (dark) patches representing the current flowing up (down), and the brightness is scaled from -2.5$\times 10^4$ to 2.5×10^4 A km^{-2}.

The spatial relations between current concentrations and flare ribbons are complicated. Flare ribbons generally appear on the edges of concentrated currents. Some flare ribbons do occur in between current concentrations of the same sign. As Canfield et al. (1992) argued, this supports a flare model of interacting flux loops, e.g., the model presented by Gold and Hoyle (1962).

The temporal relationship between current evolution and flare occurrence is revealed for the first time. Great enhancement of the line-of-sight current is
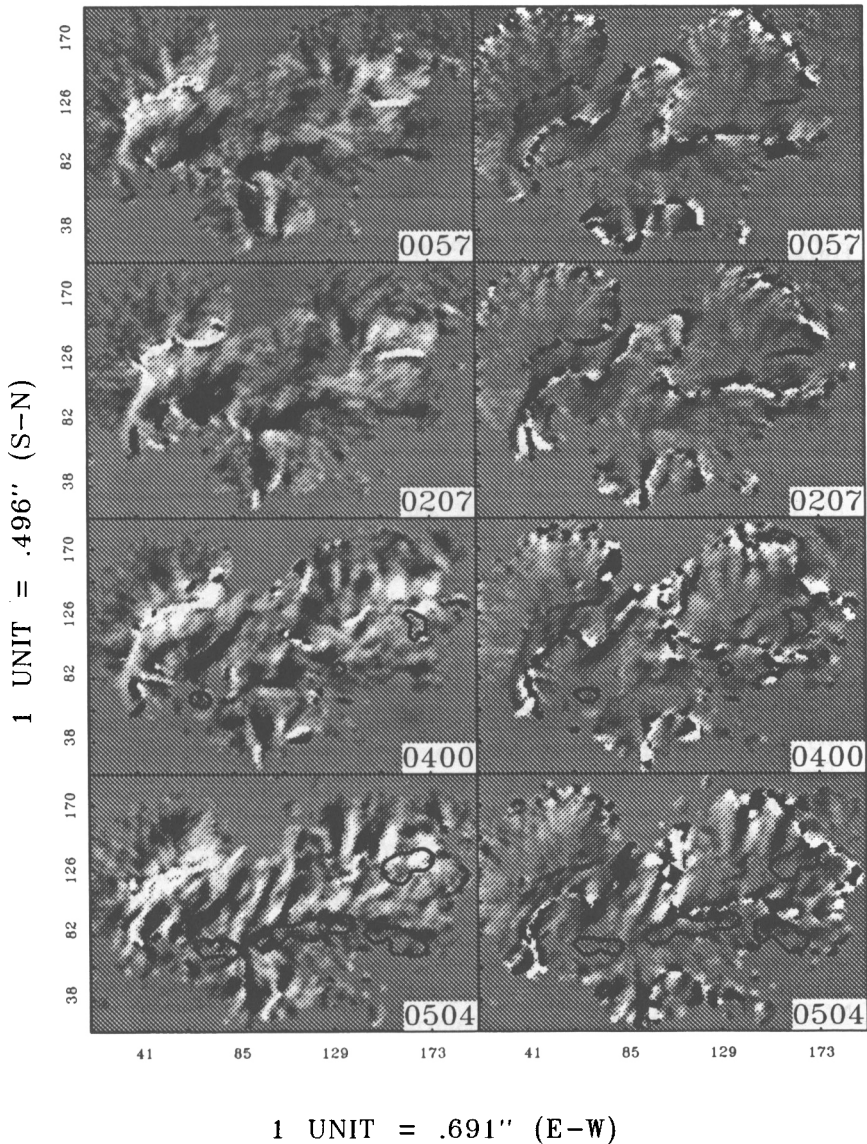
Fig. 3.   Time sequences of line-of-sight current (on the left) and force-free factor (on the right). The brightness is scaled from -2.5×10^4 to 2.5×10^4 A km^{-2} for current, and -8.5×10^{-4} to 8.5×10^{-4} km^{-1} for force-free factor. Flare ribbons are presented by isophotes.

identified preceding the 1M flare. This can be seen clearly from 00:57 to 04:00 UT in the figure. During the flare, currents reduce in magnitude, but extend in area.

As pointed out by Hagyard (1988, 1991), the source field might provide clues to identify the current path. Each set of strong source field illustrated in Figure 2 indicates a major current system flowing from concentrations of positive current to those of negative ones. The direction of the source field and the distributions of the current present a consistent picture of two major current systems in AR 6233.

3. Force-Free Factor α

The force-free factor α provides the mapping of magnetic footpoints, and the information of current helicity (Ai and Kong, 1982; Gary et al., 1987; Wilkinson, Emslie and Gary, 1989; Seehafer, 1990; Cuperman, Ofman and Semel, 1990).

In a previous study (Wang, 1992), a differential equation describing the time evolution of α has been deduced. Ignoring the Ohmic diffusion, and assuming $\nabla \cdot \vec{V} = 0$, the equation is reduced to

$$\frac{\partial \alpha}{\partial t} = \frac{1}{B^2} \vec{B} \cdot [(curl - \alpha)(\vec{B} \cdot \nabla \vec{V} - \vec{V} \cdot \nabla \vec{B})]. \tag{5}$$

This equation highlights the physics of α changes. The non-potentiality development is clearly of local nature. Many kinds of plasma motions might be as effective as shear motions in generating the magnetic shear. Moreover, it can be proved that for a large volume, the average changes of α should be zero. Starting from a potential field, a mixed sign distribution of α would be expected. The α tends to be strengthened at those sites where the gradients of magnetic and velocity fields are strongest.

By the technique suggested in section 2 above, the 2-D distribution of the force-free factor is obtained. On the right side of Figure 3, the α time sequence is shown by greyscale maps. The brightness is scaled from -8.5×10^{-4} to 8.5×10^{-4} km^{-1}. As expected, the α is highly intermittent with fully mixed signs and concentrated on the magnetic neutral line. Great enhancement is observed right before and during the 1M flare. The extreme value of α falls in the range of $\pm(5 \sim 10) \times 10^{-3}$ km^{-1}.

CONCLUDING REMARKS

(1). Current techniques might already enable an acceptable resolution of the 180 degree ambiguity in determining the direction of transverse fields.

(2). A 2-D description of angular shear is necessary for getting accurate information of the non-potentiality. The discrete FFT technique for calculating the line-of-sight current is worthy to be recommended. Consistent calibrations for B_l and B_t are essential for evaluating the source field, force-free factor, and force-free current.

(3) In the sampling region, the degree of non-potentiality quantified by all the above parameters shows great enhancement right before a major flare, then reduces somewhat slowly. Flares do appear within, or on both sides of the

extensive zones of strong angular shear, or bundles of strong source field. Flare ribbons generally appear on the edges of current concentrations.

(4) A highly intermittent force-free factor with mixed signs is obtained. This indicates that the twisting of lines of force in active regions is topologically complicated.

(5) The following efforts are of particular importance in further studies. (A) Coordinated and comparative observations with vector magnetographs and Stokes polarimeters will be of great help for a better understanding of the vector magnetogram data. (B) Complete sets of time sequences of vector magnetograms with high spatial and temporal resolution will be extremely valuable for studying the development of non-potentiality and the relationship between non-potentiality and flares. (C) A practical reconstruction of full 3-D structures of the magnetic field in active regions from the vector magnetograms is urgently needed. A non-constant force-free field is more relevant to the observations.

ACKNOWLEDGEMENT

REFERENCES

Ai, G. and Kong, F. 1982, *Acta Astronomica Sinica*, 23, 211.

Ai, G. and Hu, Y. 1986, *Publ. Beijing Astron. Obs*, 8, 1.

Ai, G., Zhang, H., Li, W., Li, J., and Chen, J. 1990, in *Solar-Terrestrial Prediction*, Proceedings of a Workshop at Leura, Australian, p.264.

Aly, J.I. 1989, *Sol. Phys.*, 120, 19.

de La Beaujardière, J-F., Canfield, R.C., and Leka, K.D. 1992, submitted to *Ap.J.*

Cacciani, A., Varsik, J., and Zirin, H. 1989, *Sol. Phys.*, 125, 173.

Canfield, R.C., Fan, Y., Leka, K.D., Mccymont, A.N., Wülser, J., Lites, B.W., and Zirin, H. 1991, *Solar Polarimetry*, ed L. November, NSO/SP Summer Workshop Series No. 11, p. 296.

Canfield, R.C., de La Beaujardière, J.-F., Fan, Y., Leka, K.D., McClymont, A.N., Metcalf, T.R., Mickey, D.L., Wülser, J-P., and Lites, B.W. 1992 submitted to *Ap. J.*

Chen, J., and Zhang, H. 1992, *Acta Astrophysica Sinica*, 12, 82.

Cuperman, S., Ofman, L., and Semel, M. 1990, *A and A*, 227, 227.

DeLoach, A.C., Hagyard, M.J., Rabin, D., Moore, R.L., Smith, J.B., Jr., West, E.A., and Tandberg-Hanssen, E. 1984, *Sol. Phys.*, 91, 235.

Ding, Y., Hagyard, M.J., Deloach, A.C., Hong, Q.F., and Liu, X.P. 1987, *Sol. Phys.*, 109, 307.

Gary, G.A., Moore, R.L., Hagyard, M.J., and Haisch, B.M. 1987, *Ap. J.*, 314, 782.

Gary, G.A. and Hagyard, M.J. 1990, *Sol. Phys.*, 126, 21.

Hagyard, M.J. 1988, *Sol. Phys.*, 115, 107.

Hagyard, M.J. 1990, *Mem. S.A.It.*, Vol.61, No.2, 337.

Hagyard, M.J., Low, B.C., and Tandberg-Hanssen, E. 1981, *Sol. Phys.*, 73, 257.

Hagyard, M.J., Smith, J.B., Jr., Teuber, D., and West, E.A. 1984, *Sol. Phys.*, 91, 115.

Hagyard, M.J., West, E.A., and Smith, J.B.,Jr. 1985, in *Proceedings of the Kunming Workshop on Solar Physics and Interplanetary Traveling Phenomena*, ed de Jagar C. and Chen, B., Science Press, Beijing, P.179.

Hagyard, M.j. and Rabin, D.M. 1986, *Adv. Space Res.*, 6, 7.

Haisch, B.M., Bruner, M.E., Harvey, M.J., and Bonnet, R.M. 1986, *AP. J.*, 300, 428.

Harvey, J.W. 1969, *Ph.D. Thesis*, Colorado University.

Ichimoto, K., Sakurai, T., Nishino, Y., Shinoda, K., Noguchi, M., Imai, H, Irie, M, Miyashita, M., Tanaka, N., and Sano, I. 1993, this volume.

Krall, K.R., Smith, J.B., Hagyard, M.J., West, E.A., and Cummings, N.P. 1982, *Sol. Phys.*, 79, 59.

Leka, K.D., Canfield, R.C., McMlymont, A.N., Fan, Y., and Tang, F. 1992, submitted to *Ap.J.*

Lin, Y. and Gaizauskas, V. 1987, *Sol. Phys.*, 109, 81.

Lin, Y., Wei, X., and Zhang, H. 1993, this volume.

Lites, B.W., Elmore, D.F., Tomczyk, S., Seagragves, P., Skumanich, A., and Streander, K.V. 1993, this volume.

Mickey, D.L., Canfield, R.C., LaBonte, B.J., and Smith, W.H. 1992, private communication.

Ming, C., Han, F., Zhang, H., Ai, G., and Kong, F. 1988, *Acta Astronomica Sinica*, 29, 346.

O'byrne, J.W., Rust, D.M., and Harris, T. 1989, *Bull AAS*, 21(2), 849.

Sakurai, T., Makita, M., and Shibasaki, K. 1985, in *Theoretical Problems in High Resolution Solar Physics*, ed. H.U. Schmidt, MPA 212, p.313.

Seehafer, N. 1990, *Sol. Phys.*, 125, 219.

Shi, Z., Wang, J., and Patterson, A. 1986, BBSO #257.

Title, A. 1993, this volume.

Wang, H. and Lin, Y. 1993, this volume.

Wang, J. 1992, *Acta Astrophysica Sinica*, 12, 75.

Wilkinson, L.K., Emslie, A.G., and Gary, G.A. 1989, *Sol. Phys.*, 119, 77.

Wu, L. 1993, this volume.

Wu, L. and Ai, G. 1990, *Acta Astrophysica Sinica*, 10, 371.